Triphenylphosphine Oxide: A Versatile Covalent Functionality for Carbon Nanotubes

GDCh Research Article Angewandte International Edition Chemie www.angewandte.org

How to cite: Angew. Chem. Int. Ed. 2024, e202412084
doi.org/10.1002/anie.202412084

Nanotubes Hot Paper

Triphenylphosphine Oxide: A Versatile Covalent Functionality for Carbon Nanotubes

*Yanlin Pan, Dominika Baster, Daniel Käch, Jan Reger, Lionel Wettstein, Frank Krumeich, Mario El Kazzi, and Máté J. Bezdek**

Dedicated to Prof. Dr. Hansjörg Grützmacher on the occasion of his 65th birthday.

Abstract: Broadening the scope of functionalities that can be covalently bound to single-walled carbon nanotubes (SWCNTs) is crucial for enhancing the versatility of this promising nanomaterial class in applied settings. Here we report the covalent linkage of triphenylphosphine oxide [$Ph_3P(O)$] to SWCNTs, a hitherto overlooked surface functionality. We detail the synthesis and structural characterization of a new family of phosphine oxide-functionalized diaryliodonium salts that can facilitate direct $Ph_3P(O)$ transfer and afford novel SWCNTs with tunable $Ph_3P(O)$ content (**SWCNT-P**). The molecularly-distributed and robust nature of the covalent $Ph_3P(O)$ attachment in **SWCNT-P** was supported by a combination of characterization methods including Raman, infrared, UV/Vis-NIR and X-ray photoelectron spectroscopies coupled with thermogravimetric analysis. Electron microscopy further revealed the effectiveness of the $Ph_3P(O)$ moiety for de-bundling SWCNTs to yield **SWCNT-P** with superior dispersibility and processability. Finally, electrochemical studies established that **SWCNT-P** is sensitive to the presence of Li^+, Na^+ and K^+ wherein the Gutmann-Beckett Lewis acidity parameters of the ions were quantitatively transduced by $Ph_3P(O)$ to electrochemical responses. This work hence presents a synthetic, structural, spectroscopic and electrochemical foundation for a new phosphorus-enriched responsive nanomaterial platform featuring the $Ph_3P(O)$ functionality.

[*] Y. Pan, D. Käch, J. Reger, L. Wettstein, Dr. F. Krumeich, Prof. Dr. M. J. Bezdek
Department of Chemistry and Applied Biosciences
ETH Zürich
Vladimir-Prelog-Weg 1, 8093 Zürich, Switzerland
E-mail: mbezdek@ethz.ch

Dr. D. Baster, Dr. M. El Kazzi
PSI Center for Energy and Environmental Sciences
Paul Scherrer Institute
Forschungsstrasse 111, 5232, Villigen, Switzerland

Introduction

Owing to their unique physical, mechanical and electronic properties, single-walled carbon nanotubes (SWCNTs) are emerging as next-generation building blocks for sensors,[1] energy storage systems,[2] biomedical devices,[3] heterogeneous catalysts,[4] and advanced electronic materials.[5] Given the variety of settings in which SWCNTs find utility, the ability to tailor their physical and chemical properties to the desired application is critical. Accordingly, methods for the atomically precise introduction of functionalities to predictably tune SWCNT surface chemistry, processability, and electronic transport characteristics continue to attract significant research interest.[5a]

As a complementary approach to the non-covalent functionalization[6] and the mechanical interlocking of SWCNTs,[7] direct covalent modification[8] offers expedient access to functional carbon nanotubes exhibiting long-term stability. As shown in Scheme 1A (top), SWCNTs can be covalently functionalized using approaches that include halogenation,[9] alkylation/arylation,[10] radical coupling,[11] cycloaddition,[12] or nitrene addition reactions.[13] However, given the difficulty of bond formation at the extended π-sidewalls of SWCNTs and their poor processability,[14] such protocols require reaction conditions that limit the scope of functional groups that can be installed and hence constrain subsequent applications. This drawback can be partly overcome by utilizing a surface "linker"[15] group to immobilize functionalities through stepwise reactions (Scheme 1A, bottom). However, the heterogeneous nature of SWCNTs often renders such multi-step methods cumbersome. Further, the use of linker groups often interrupts electronic communication between the surface functionality and the SWCNTs that hampers the utility of the resulting nanomaterial in applications that rely on their electronic coupling.[16] Consequently, atomically precise methods are needed that can directly introduce new functionalities in the immediate vicinity of the SWCNT surface to unlock their full potential in electronic materials applications.

In this work, we pursue a strategy to covalently install the triphenylphosphine oxide functionality [$Ph_3P(O)$] on SWCNTs to access a new class of phosphorus-enriched nanomaterials (**SWCNT-P**, Scheme 1B). We were drawn to the $Ph_3P(O)$ moiety for several reasons. First, $Ph_3P(O)$ is a potentially versatile yet essentially unexplored functionality for SWCNT surface chemistry with intriguing

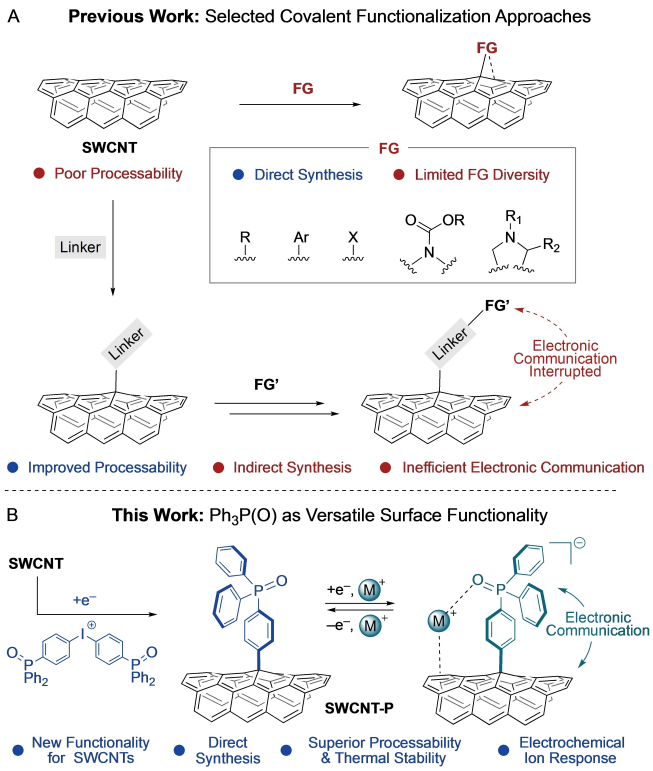

Scheme 1. (A) Selected approaches for the covalent functionalization of single-walled carbon nanotubes (SWCNTs). (B) The strategy reported in the present study. FG = functional group. $M^+ = Li^+$, Na^+ and K^+.

optoelectronic[17] and physical[18] properties. Moreover, phosphine oxides are sufficiently robust to be incorporated into direct SWCNT functionalization schemes. Importantly, the steric profile of a surface $Ph_3P(O)$ group is expected to disrupt inter-SWCNT interactions, thereby leading to improved dispersibility properties for the functionalized nanomaterial that is crucial for materials processing in applied settings.[19] Finally, given the ability of phosphine oxides to interact with ions,[20] we reasoned that covalently immobilizing $Ph_3P(O)$ in the proximity of the SWCNT sidewall would give rise to ion-responsive properties that could be leveraged in functional materials applications.

Herein we realize these goals and demonstrate that triphenylphosphine oxide is a versatile surface functionality for SWCNTs. To this end, we detail the synthesis and structural characterization of a new family of phosphine oxide-functionalized diaryliodonium salts that can undergo $Ph_3P(O)$-transfer upon single-electron reduction and furnish novel, covalently modified SWCNTs with tunable $Ph_3P(O)$ content. We characterize **SWCNT-P** by a suite of spectroscopic methods, electron microscopy as well as thermogravimetric analysis to examine the influence of the $Ph_3P(O)$ functionality on the electronic and physical properties of this new phosphorus-enriched nanomaterial. Finally, we show that **SWCNT-P** exhibits an electrochemical response that can be correlated with the Lewis acidity of ions in its proximity, establishing $Ph_3P(O)$ as an effective probe for transducing chemical information into an electronic signal.

Results and Discussion

Synthesis and Characterization of Phosphine Oxide-Functionalized Iodonium Reagents

Our studies commenced with the synthesis of a reagent suitable for transferring the $Ph_3P(O)$ functionality to SWCNTs. In this pursuit, we were inspired by previous reports on the use of diaryliodonium salts ($[Ar_2I]^+$) as conveniently-handled sources of reactive aryl radicals (Ar•).[21] Upon single-electron reduction, $[Ar_2I]^+$ reagents undergo homolytic C–I bond cleavage and the concomitantly generated Ar• can form covalent bonds with carbon nanomaterials. Accordingly, we targeted the synthesis of diaryliodonium species bearing phosphine oxide functionalities using the two parallel strategies shown in Scheme 2. Specifically, we aimed to synthesize both "unsymmetrical" and "symmetrical" diaryliodonium salts that are expected to have different efficiencies of phosphine oxide-functionalized aryl radical generation upon reduction. Hence, such reagents can potentially offer fine control over the degree of $Ph_3P(O)$ incorporation in SWCNTs.

Shown in Scheme 2 (top), stepwise treatment of (4-iodophenyl)diphenylphosphine oxide $[(C_6H_4I)(Ph)_2P(O)]$ with triflic acid, followed by the addition of *m*-CPBA and 1,3,5-triisopropylbenzene $[(i\text{-}Pr)_3C_6H_3]$ afforded the iodonium salt **1** in 74% yield after heating at 50 °C for 16 h. For the synthesis of the symmetrical variant, oxidation to iodine(III) was accomplished with *m*-CPBA in the presence of $BF_3{\cdot}OEt_2$ while subsequent C–I bond formation was achieved upon addition of borylated triphenylphosphine oxide and stirring at 50 °C for 24 hours (Scheme 2, bottom). The ^1H and $^{31}P\{^1H\}$ NMR spectra of **1** and **2** exhibit the number of peaks consistent with overall C_s and C_{2v} molecular symmetries in solution, respectively. The electron-withdrawing nature of the $Ph_3P(O)$ moiety relative to $[(i\text{-}Pr)_3C_6H_3]$ was indicated by shifting of the arene *C–H* resonances *ortho* to iodine from 8.03 ppm in **1**, to 8.39 ppm in the case of **2** (DMSO-d_6). In this regard, the isolation of **2** is especially noteworthy given that the synthesis of sym-

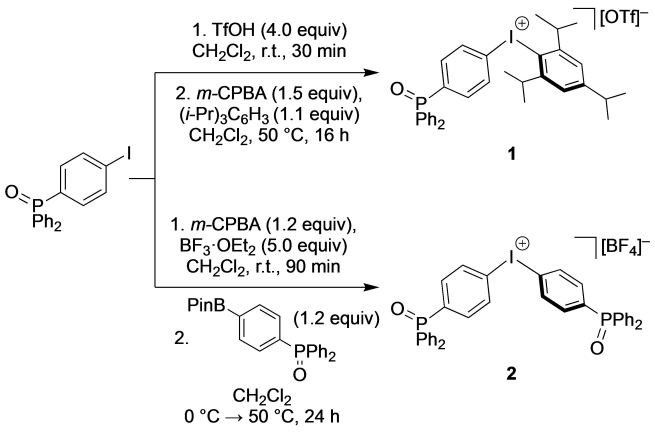

Scheme 2. Syntheses of diaryliodonium salts **1** (top) and **2** (bottom). Pin = pinacolato.

metrical iodonium salts bearing electron-withdrawing substituents is considered challenging.[22]

The solid-state structures of iodonium salts **1** and **2** were determined by single-crystal X-ray diffraction.[23] Shown in Figure 1, the solid-state packing of both compounds is governed by intermolecular halogen bonds (XBs),[24] with iodine and phosphine oxide serving as the XB donor[25] and acceptor,[26] respectively. The intermolecular I···O contacts for both **1** and **2** are significantly below the sum of the van der Waals radii of the two atoms ($d_{I\cdots O}$ = 2.65–2.85 Å; Σr_{vdW} = 3.5 Å)[27] and, together with the observation of nearly straight C–I···O angles (174.61–175.04°), serve as diagnostic XB indicators. While iodine forms a single XB opposite to the [(*i*-Pr)$_3$C$_6$H$_2$] moiety in **1**, the formation of two XBs are observed in the vicinity of iodine in the case of **2**. These bonding preferences result in distinct solid-state packing scenarios for the two compounds, wherein a ribbon-like 1D chain is formed for **1** (Figure 1B), and **2** is assembled into a 2D network (Figure 1D). These observations demonstrate that the Ph$_3$P(O) moieties are responsible for directing the supramolecular architectures of the iodonium salts via intermolecular XB formation.

A notable difference between the structural metrics of the two iodonium salts is the observation of shorter I···O contacts for **2** compared to **1**, a qualitative indicator of relatively stronger XB strength.[26c,e] In addition, a C···O interaction (3.103(5) Å) within Σr_{vdW} (3.2 Å) between the aryl *ipso*-carbon adjacent to iodine and a phosphine oxide is observed in the solid-state structure of **2** (C19–O1', Figure 1C). These observations can be rationalized by the enhanced iodine electrophilicity that results from the presence of two, rather than one, electron-withdrawing[28] triarylphosphine oxide functionalities in **2**. Interestingly, while the phosphine oxide functionality *intra*molecularly gives rise to an iodine center with enhanced electrophilicity in **2**, its polarized P–O bonds[29] are nucleophilic at oxygen

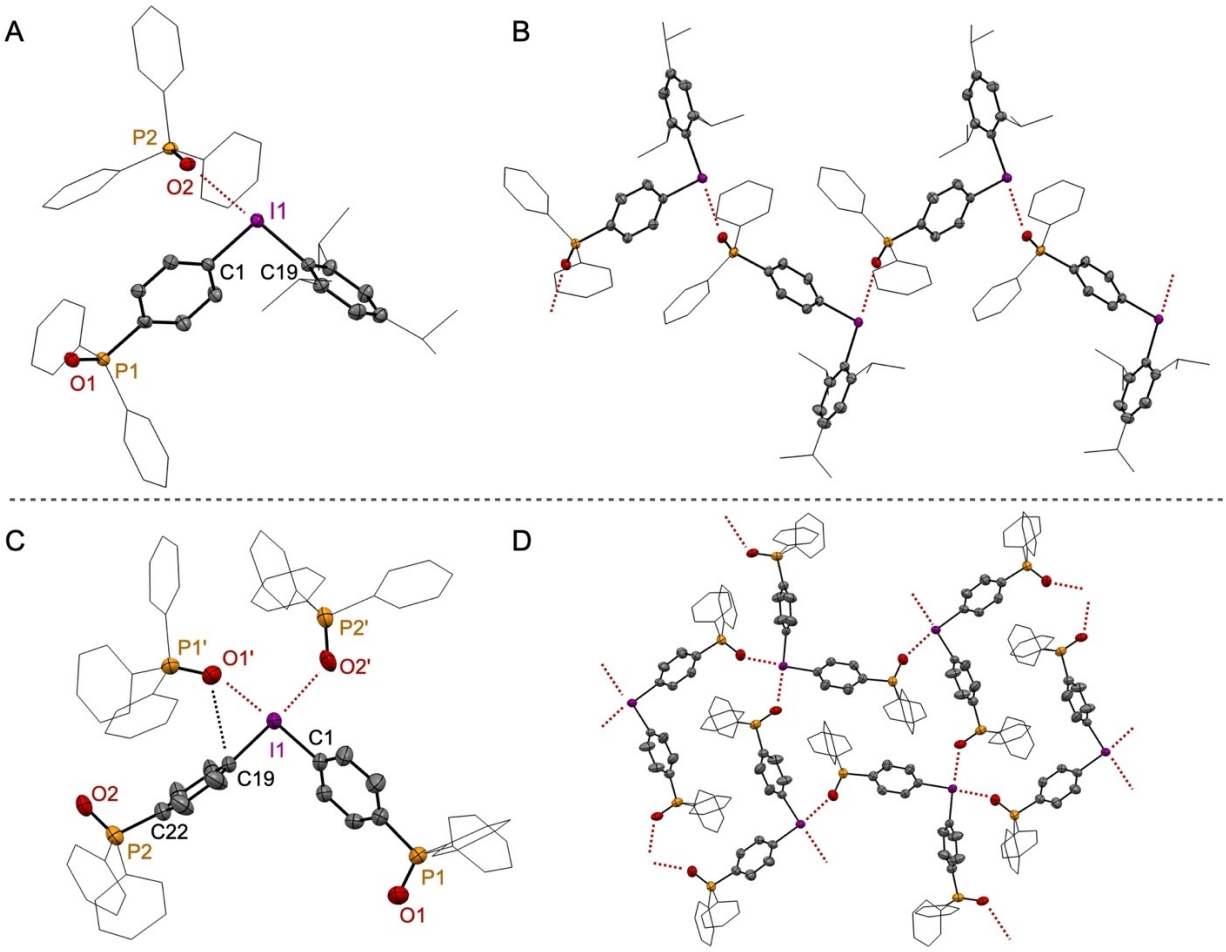

Figure 1. (A) Solid-state structure of **1**. A triarylphosphine oxide moiety belonging to a crystallographically independent molecule of **1** in the unit cell has been depicted to illustrate intermolecular halogen bonding (red dashed line). Selected bond lengths (Å) and angles (deg): I1–C1 2.127(3), I1–C19 2.123(8), I1–O2 2.814(3), P1–O1 1.497(7), C19–I1–O2 174.85(10). (B) Solid-state packing of **1**. (C) Solid-state structure of **2**. Two triarylphosphine oxide moieties belonging to symmetry-generated molecules of **2** in adjacent unit cells have been depicted to illustrate intermolecular halogen bonding (red dashed lines). Selected bond lengths (Å) and angles (deg): I1–C1 2.104(4), I1–C19 2.107(4), I1–O1' 2.652(4), I1–O2' 2.724(4), C19–O1' 3.103(5), P1–O1 1.470(4), P2–O2 1.490(4), C1–I1–O1' 174.61(13), C19–I1–O2' 175.04(14). (D) Solid-state packing of **2**. All structures are represented with 50% probability ellipsoids. Hydrogen atoms and counterions have been omitted, while phenyl and isopropyl substituents are represented without probability ellipsoids for clarity.

and serve as effective XB acceptors, thus providing *inter*molecular stabilization. To our knowledge, compounds **1** and **2** represent the first structurally characterized examples of a phosphine oxide moiety participating in halogen bonding with a diaryliodonium center[30] and underscore the propensity of the $Ar_3P(O)$ functionality to interact with, and stabilize cations.[20] Leveraging this feature for bulk material function is described in greater detail below.

Direct Covalent SWCNT Functionalization

With a pair of iodonium salts bearing phosphine oxides in hand, their utility in covalent SWCNT functionalization was examined. In a typical procedure, purified SWCNTs (6,5 chirality enriched) were first dispersed in THF and treated with sodium naphthalenide reductant ($Na[C_{10}H_8]$) to achieve exfoliation and conversion to a reactive, polyanionic state.[31] Iodonium salts **1** or **2** were then added, and the dispersion was stirred for 16 h at room temperature to accomplish $Ph_3P(O)$ transfer via reduction and radical fragmentation of the iodonium reagent (Scheme 3A). The extent of covalent modification in **SWCNT-P** was assessed by examining the area ratio of the D- and G-bands in the Raman spectrum of the product film at ca. 1297 cm^{-1} and 1589 cm^{-1}, respectively. This ratio (A_D/A_G) is a convenient handle for evaluating covalent surface functionalization in graphitic nanomaterials, wherein the conversion of sp^2 carbon atoms into sp^3 sites upon σ-bond formation increases the D-band intensity due to symmetry-breaking, defect-induced Raman scattering.[32] Indeed, the procedure outlined in Scheme 3A prominently increased the A_D/A_G ratio that signaled the successful covalent bond formation at the carbon nanotube surface in **SWCNT-P** (Scheme 3B).

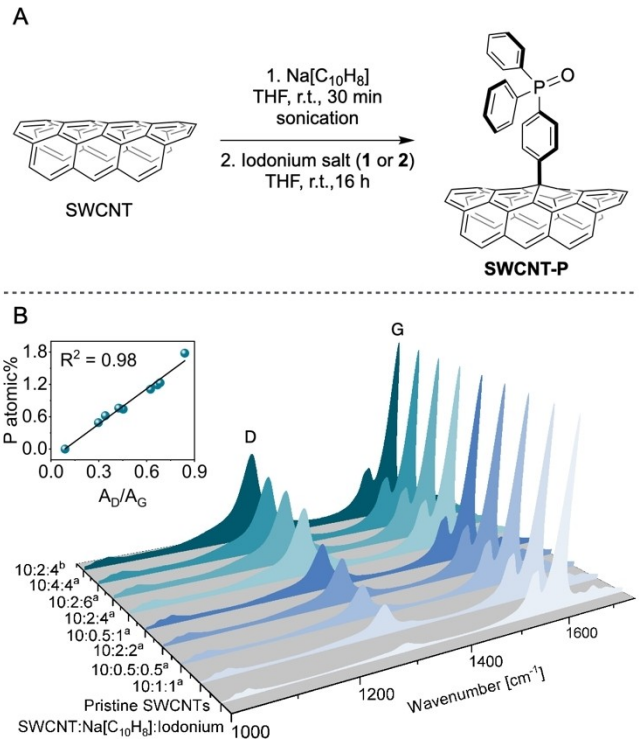

Scheme 3. (A) Synthesis of $Ph_3P(O)$-functionalized carbon nanotubes (**SWCNT-P**). (B) Raman spectra of **SWCNT-P** synthesized using various starting material ratios. [a] Iodonium salt **1**. [b] Iodonium salt **2**. Inset: Correlation between XPS phosphorus content (P atomic %) and the D-band to G-band ratio (A_D/A_G) determined by Raman spectroscopy (633 nm laser excitation) for **SWCNT-P**.

Shown in Scheme 3B, systematic variation of the relative ratios of SWCNT, reductant and iodonium salt (**1** or **2**) resulted in adjustable extent of nanotube sidewall functionalization with A_D/A_G values between 0.297 and 0.839 (A_D/A_G for pristine SWCNTs = 0.088). To confirm the surface composition of the functionalized SWCNTs, X-ray photoelectron spectroscopy (XPS) was performed on **SWCNT-P** and showed peaks corresponding to C 1s, O 1s and P 2p binding energies at 284.7, 530.5 and 132.1 eV, respectively (Figure S17).[33] A linear correlation was found between A_D/A_G and the surface phosphorus content (atom %) in **SWCNT-P** that supports the presence of a phosphine oxide functionality at each $C(sp^3)$ defect (Scheme 3B inset and Table S1). This linear relationship between A_D/A_G and surface P content provides an accessible handle for quantifying $C(sp^3)$ defect density by Raman spectroscopy,[34] which typically represents an analytical challenge for SWCNTs with a high degree of surface functionalization. In addition, the linear correlation argues against polyaryl growth at the solution-SWCNT interface, a common side reaction hindering many covalent functionalization protocols that proceed via reactive aryl radical intermediates.[11,21d] Importantly, an approximately 1:1 ratio was found by XPS between the surface oxygen and phosphorus content in **SWCNT-P** irrespective of the overall degree of functionalization, consistent with the presence of well-defined $Ph_3P(O)$ moieties on the SWCNT surface (Table S5).

The results presented in Scheme 3B demonstrate that while both iodonium salts **1** and **2** can be used to install $Ph_3P(O)$ functionalities on SWCNTs, the highest surface phosphorus content was achieved with **2**. The higher SWCNT functionalization efficiency of **2** may be rationalized considering electronic factors. Previous studies have shown that diaryliodonium salts bearing electron-withdrawing aryl substituents can be reduced at milder potentials and can generate reactive Ar• more readily compared to those bearing electron-donating groups.[35] Thus, relative Ar_2I^+ electrophilicity can be correlated with covalent functionalization efficiency. Indeed, the solid-state structural analysis presented above is consistent with iodonium **2** exhibiting greater electrophilicity compared to **1**. The stronger electron-withdrawing ability[36] of $Ar_3P(O)$ versus $[(i\text{-}Pr)_3Ar]$ likely translates to a positively shifted reduction potential[37] for **2** relative to **1** and may hence contribute to its greater efficiency of $Ph_3P(O)$-transfer. Besides electronic considerations, the presence of two $Ar_3P(O)$ functionalities per molecule of **2** also results in an increased statistical likelihood of phosphine oxide-functionalized Ar• generation compared to **1**.[38] The highest level of surface functionalization achieved with **2** (1.78 %) corresponds approximately to 1 $Ph_3P(O)$ unit per 50 SWCNT carbon atoms, or 14 hexagonal "rings" in 6,5-SWCNTs (as drawn in Scheme 3A). The

successful and controlled synthesis of **SWCNT-P** motivated further experiments to gain deeper insight into its solid-state properties.

Shown in Figure 2, **SWCNT-P** was characterized by a suite of spectroscopic methods. High-resolution XPS spectra of **SWCNT-P** showed the presence of peaks assignable to P $2p_{1/2}$ and P $2p_{3/2}$ binding energies at 133.0 and 132.2 eV, respectively, consistent with the presence of surface phosphorus(V) species (Figure 2A).[33] Further, infrared (IR) spectroscopy allowed the identification of the P–O vibrational frequency at 1197 cm^{-1} for the phosphine oxide moiety in the solid-state (Figure 2B).[39] The optical absorption of a **SWCNT-P** dispersion was evaluated by UV/Vis-NIR spectroscopy and showed the characteristic features of semiconducting carbon nanotubes with interband transitions of van Hove singularities in the 800–1300 nm (S_{11}) and 500–750 nm (S_{22}) regions as shown in Figure 2C.[40] Importantly, the broadening and attenuation of absorption features in **SWCNT-P** relative to pristine nanotubes is consistent with the formation of surface C(sp^3) sites that perturb π-conjugation rather than functional group physisorption.[11c] The partial retention of features in the S_{11} and S_{22} regions for **SWCNT-P** nevertheless indicates that the optoelectronic properties of semiconducting SWCNTs can be preserved following controlled covalent functionalization.[41]

To evaluate whether the $Ph_3P(O)$ functionalities are uniformly distributed on the carbon nanotube surface, a series of Raman spectra were collected for a larger sample area in **SWCNT-P** (50×60 μm). The subsequent construction of a 2D map showed a relatively small variation in A_D/A_G values and hence a uniform distribution of C(sp^3) sites (Figure 2D). **SWCNT-P** was then imaged by scanning transmission electron microscopy (STEM) and a map of key elements was visualized by energy dispersive X-ray spectroscopy (EDXS). Displayed in Figure 2E, STEM-EDXS showed spatial correlation between carbon, oxygen and phosphorus content in **SWCNT-P**. Further, STEM-EDXS data collected at multiple film locations showed no significant variation of elemental composition (Figure S12). Taken together, these data support the notion that covalently bound $Ph_3P(O)$ functionalities are molecularly distributed in the **SWCNT-P** film.

An anticipated advantage of the covalently installed $Ph_3P(O)$ functionality was the disruption of intertube interactions which otherwise hinder the dispersibility and therefore the processability of pristine SWCNTs. High-resolution transmission electron microscopy (HRTEM) was hence employed to obtain images of **SWCNT-P** nanotube bundles which showed an average intertube distance of 0.28 ± 0.06 nm ($N = 10$; Figures 3A and S14). This value is larger than the intertube distance of pristine SWCNT bundles determined by HRTEM (0.15 ± 0.04 nm, $N = 10$; Figure S13) which suggests a de-bundling effect of the surface $Ph_3P(O)$ functionality. These observations were further supported by scanning electron microscopy (SEM), which showed a reduced average bundle size for **SWCNT-P**

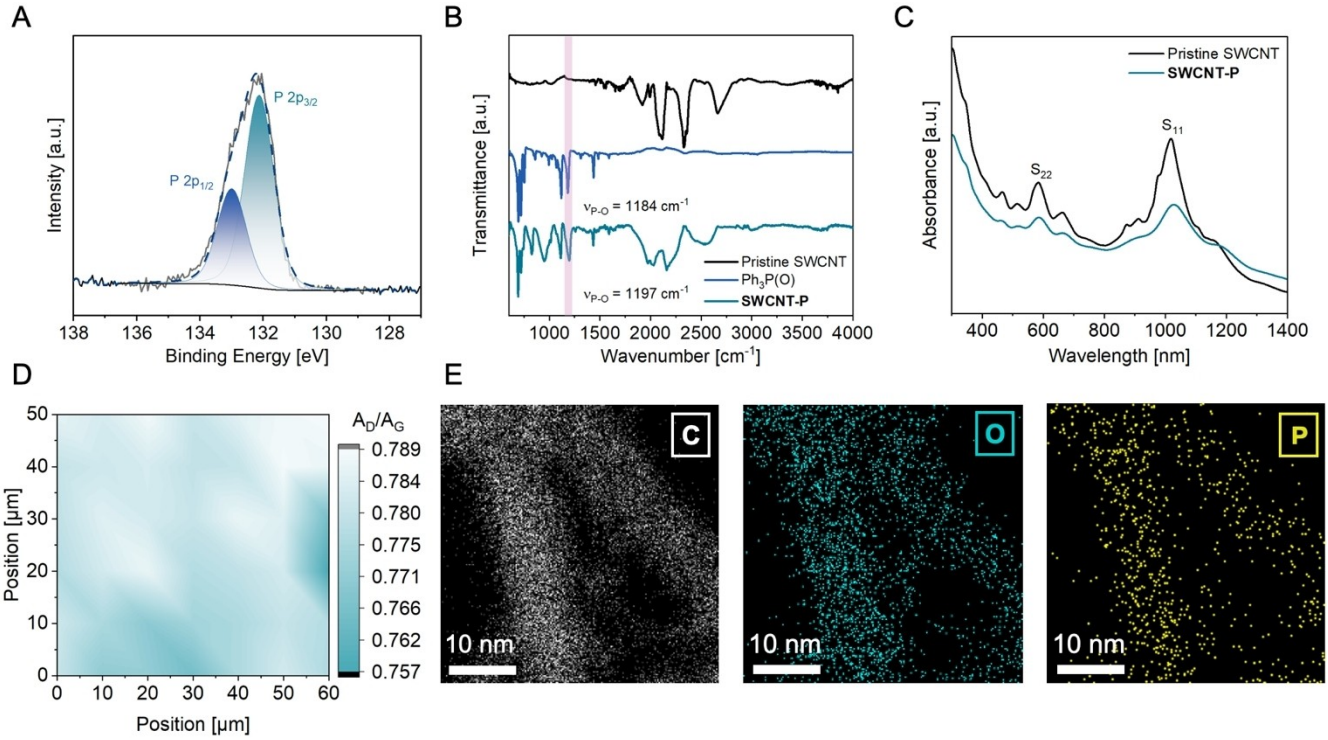

Figure 2. (A) High-resolution P 2p XPS spectrum of **SWCNT-P**. (B) IR spectra of pristine SWCNTs (black, top), $Ph_3P(O)$ (blue, middle) and **SWCNT-P** (petrol, bottom). (C) UV/Vis-NIR spectra of pristine SWCNT (black) and **SWCNT-P** (petrol). (D) Raman A_D/A_G map of a **SWCNT-P** film (633 nm laser excitation). (E) STEM-EDXS images of **SWCNT-P**, false-colored for elemental mapping in white (carbon), blue (oxygen, sample contains residual SiO_2) and yellow (phosphorus), ($U_{acc} = 80$ kV).

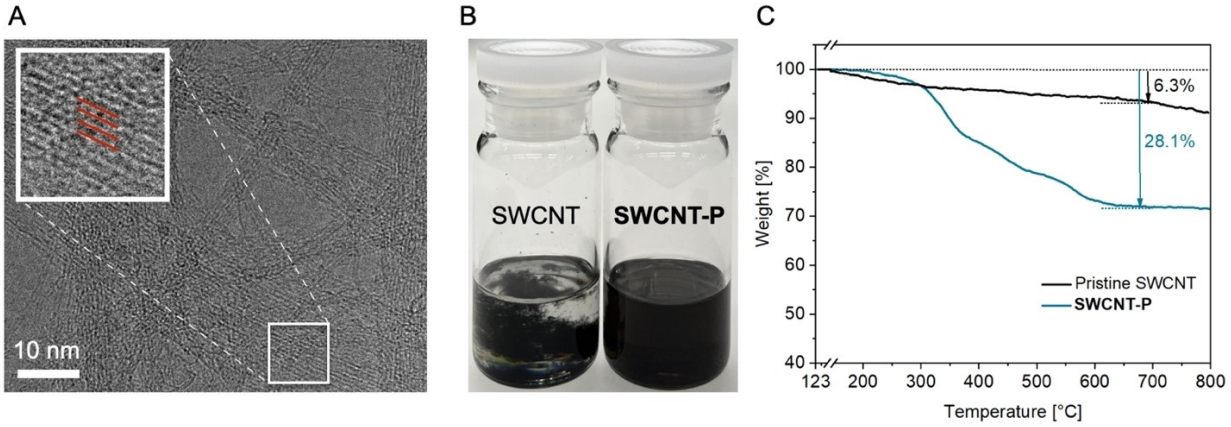

Figure 3. HRTEM image of drop-cast **SWCNT-P** (U_{acc} = 300 kV). Inset: enlargement at higher magnification showing periodic SWCNT fringes (highlighted with red lines). B) Photograph of dispersions of pristine SWCNTs and **SWCNT-P** in *o*-DCB (20 mg/L). C) TGA curves of pristine SWCNT (black) and **SWCNT-P** (petrol).

compared to pristine SWCNTs (Figure S11). This attribute likely underpins the superior stability of **SWCNT-P** dispersions, which can be obtained in *ortho*-dichlorobenzene (*o*-DCB) at a concentration of 20 mg/L upon mild sonication (Figure 3B). In contrast to pristine SWCNTs that begin to aggregate in *o*-DCB at comparable concentrations, **SWCNT-P** dispersions are stable for several months without added surfactants and present a clear advantage for nanomaterial processing.

In addition to its stability as a dispersion, the thermal stability of **SWCNT-P** films was also evaluated. For this purpose, thermal gravimetric analysis (TGA) was performed and revealed ca. 28.1 % mass loss in **SWCNT-P** upon heating to 700 °C (Figure 3C, Table S3). This value is significantly higher than 6.3 % mass loss observed for pristine SWCNTs in the same temperature range and is consistent with the presence of surface functionalities in **SWCNT-P**. Importantly, no $Ph_3P(O)$-derived volatile decomposition products were detectable below 400 °C by TGA/mass spectrometry, with mass loss below this temperature assigned primarily to solvent evaporation and degassing (Figures S6, S7).[13b] This observation underscores the enhanced thermal stability[42] of $Ph_3P(O)$ compared to other surface functionalities such as aryl groups and rules out the presence of physiosorbed unreacted iodonium salts (Figure S9). Following TGA analysis of **SWCNT-P** (i.e. after heating to 800 °C then cooling to r.t.), its Raman spectrum was restored to that observed for pristine SWCNTs, indicating that the nanotube aspect ratios generally remain unchanged during functionalization and do not fragment (Figure S4). Overall, the TGA data are consistent with the formation of thermally robust covalent linkages between the $Ph_3P(O)$ functionalities and the SWCNT sidewall.

Electrochemical Ion Response

The successful covalent attachment of the robust $Ph_3P(O)$ functionality presented an opportunity to explore the application of **SWCNT-P** as an ion-responsive material. We selected electrochemistry for this purpose due to its utility as a simple and low-cost analytical method that is sensitive to processes occurring on the surfaces of conductive materials.[43] To this end, **SWCNT-P** was dispersed and drop-cast onto a glassy carbon working electrode surface (7.1 mm^2) and its electrochemical behavior was examined by cyclic voltammetry. Shown in Figure 4A, the cyclic voltammogram (CV) of **SWCNT-P** exhibits a characteristic "dumbbell" shape with anodic and cathodic current inflections at −0.08 V (E_A) and −0.29 V (E_C) vs Fc/Fc^+, respectively. A linear dependence of peak current on scan rate was observed during the electrochemical charging of **SWCNT-P**, evidencing surface-confined rather than solution-based electrochemical events (Figure S24–S27).[44] Based on the reported electrochemical behavior of carbon nanotubes, **SWCNT-P** is assumed to be quantum capacitance-dominated wherein the applied potential induces a Fermi level shift in the nanomaterial and the measured currents are

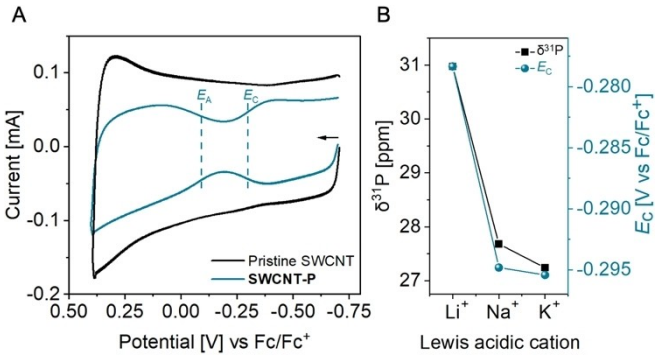

Figure 4. A) CVs of pristine SWCNTs (black) and **SWCNT-P** (petrol) drop-cast on glassy carbon working electrode at 100 $mV\,s^{-1}$ (r.t., 0.1 M $[(n\text{-}Bu)_4N][PF_6]$ in MeCN). B) Correlation between E_C of **SWCNT-P** in the presence of cations (petrol) and the corresponding Gutmann-Beckett Lewis acidity parameters of the ions ($\delta^{31}P$, black). Data for $\delta^{31}P$ from ref. [20a].

correlated with increases in the density of its fully occupied or empty states.[45] These states are either depleted or filled with electrons upon the application of positive or negative potential, respectively. The difference between E_A and E_C can then be used to estimate the band gap of the carbon nanomaterial.[46] In contrast to the relatively narrow spacing between the cathodic and anodic features for **SWCNT-P** ($|E_A - E_C| \approx 0.21$ V), a wider potential window between cathodic and anodic events was observed for pristine SWCNTs (Figure S23). These observations suggest that covalent attachment of the $Ph_3P(O)$ functionality likely gives rise to midgap "defect" states in the SWCNT band structure, yielding a smaller electrochemical band gap.[47]

The distinct and clearly defined anodic and cathodic onset potentials observed for **SWCNT-P** led us to investigate whether altering its chemical environment would produce an electrochemical response detectable by changes in its CV. Given the propensity of $Ph_3P(O)$ to interact with cations,[20] the CV of **SWCNT-P** was thus evaluated in the presence of 0.1 M $Li[PF_6]$, $Na[PF_6]$ and $K[PF_6]$ supporting electrolytes. The inflection of the **SWCNT-P** cathodic potential (E_C) showed a consistent trend across independent electrochemical experiments for the alkali metal series wherein Li^+ gave rise to the most positive value followed by Na^+ and K^+ (Table S6). Strikingly, the observed E_C values for **SWCNT-P** in the presence of Li^+, Na^+ and K^+ were found to correlate closely with the relative differences in solution-phase Gutmann-Beckett Lewis acidities of the alkali metal ions (Figure 4B).[20a] By stark contrast, control experiments established no statistically distinguishable trend in E_C for pristine SWCNTs with the same ion series (Figure S22A). These observations indicate that $Ph_3P(O)$ groups and the SWCNTs are electronically coupled wherein an ion binding event likely manifests in the measured E_C values.

The electrochemical ion response presented in Figure 4B is remarkable considering that the electrode surface loading density of $Ph_3P(O)$ in **SWCNT-P** is approximately 1 *nano*-moles mm^{-2} and shows that $Ph_3P(O)$ is capable of quantitatively translating information about its chemical environment into an electronic signal. It is important to note that the response was achieved using an overall simple system, without a redox-active, transition metal-based signaling molecule on the SWCNT surface.[48] The use of a conventional electrochemical setup in our experiments further underscores the possibility of electronic signal transduction using **SWCNT-P** which obviates the need for cumbersome and expensive analytical instrumentation. The exceptional combination of thermal stability, superior dispersibility and ion-interaction ability of **SWCNT-P** thus serves as a key proof-of-concept and establishes phosphine oxide-functionalized SWCNTs as a promising new class of responsive nanomaterials.

Conclusions

In summary, we demonstrated the direct covalent attachment of triphenylphosphine oxide to SWCNTs. A new family of phosphine oxide-functionalized diaryliodonium salts was synthesized, structurally characterized, and applied as $Ph_3P(O)$-transfer reagents to achieve the covalent modification of SWCNTs using a direct, single-step procedure. The resulting **SWCNT-P** nanomaterial was characterized by a wide array of spectroscopic methods, electron microscopy, as well as thermogravimetric analysis which established the unique influence of $Ph_3P(O)$ on the physical and electronic properties of the SWCNTs. Finally, electrochemical studies showed that the electronic coupling between the $Ph_3P(O)$ moiety and the carbon nanotubes can be leveraged to translate Lewis acidity parameters of ions in its proximity into an electrochemical response. Besides application as ion-responsive probes,[48] we envision that the phosphorus-rich SWCNTs reported herein may serve as a general platform for next-generation electronic materials, supported (electro)catalysts,[49] element recycling schemes,[20d,50] optical sensors,[8c] spintronics,[51] and energy storage media.[52] Additionally, functionalized diaryliodonium salts may be applied in synthesis as convenient phosphine oxide transfer reagents.[53] Given these prospects, our investigations open new parameter space for exploration in the realms of functional molecules and materials using the commonly overlooked yet versatile $Ph_3P(O)$ functionality.

Acknowledgements

ETH Zürich and the Swiss National Science Foundation (SNSF 207390) are thanked for financial support. Y. L. P thanks the Chinese government for a CSC scholarship (202209210015). The Molecular and Biomolecular Analysis Service (MoBiAS), X-ray (SMoCC) and NMR facilities of ETH Zürich are acknowledged for technical assistance. Dr. Hartmut Schönberg and Dr. Debora Thöny (ETH Zürich) are thanked for assistance with TGA/MS data collection. The authors also thank Fabio Masero and Dr. Sergii Yakunin (ETH Zürich) for assistance with measurement of Raman and NIR emission data, respectively. Prof. Dr. Antonella Rossi Elsener (ETH Zürich) is thanked for insightful discussions. Open Access funding provided by Eidgenössische Technische Hochschule Zürich.

Conflict of Interest

The authors declare no conflict of interest.

Data Availability Statement

The data that support the findings of this study are available in the supplementary material of this article.

Keywords: nanotubes · phosphine oxides · iodonium salts · electrochemistry · ion-responsive nanomaterials

[1] a) J. Kong, N. R. Franklin, C. Zhou, M. G. Chapline, S. Peng, K. Cho, H. Dai, *Science* **2000**, *287*, 622–625; b) V. Schroeder, S. Savagatrup, M. He, S. Lin, T. M. Swager, *Chem. Rev.* **2019**, *119*, 599–663.

[2] a) W. Pan, Y. Zhao, J. Mao, Y. Wang, X. Zhao, K. W. Leong, S. Luo, X. Liu, H. Wang, J. Xuan, S. Yang, Y. Chen, D. Y. C. Leung, *Adv. Energy Mater.* **2021**, *11*, 2101514, https://doi.org/10.1002/aenm.202101514; b) L. Ye, M. Liao, H. Sun, Y. Yang, C. Tang, Y. Zhao, L. Wang, Y. Xu, L. Zhang, B. Wang, F. Xu, X. Sun, Y. Zhang, H. Dai, P. G. Bruce, H. Peng, *Angew. Chem. Int. Ed.* **2019**, *58*, 2437–2442; c) B. J. Landi, M. J. Ganter, C. D. Cress, R. A. DiLeo, R. P. Raffaelle, *Energy Environ. Sci.* **2009**, *2*, 638–654.

[3] a) D. A. Heller, S. Baik, T. E. Eurell, M. S. Strano, *Adv. Mater.* **2005**, *17*, 2793–2799; b) Z. Liu, S. Tabakman, K. Welsher, H. Dai, *Nano Res.* **2009**, *2*, 85–120; c) H. Wang, N. B. Muren, D. Ordinario, A. A. Gorodetsky, J. K. Barton, C. Nuckolls, *Chem. Sci.* **2012**, *3*, 62–65.

[4] a) T. Kitanosono, P. Xu, S. Kobayashi, *Science* **2018**, *362*, 311–315; b) M. Blanco, B. Nieto-Ortega, A. de Juan, M. Vera-Hidalgo, A. López-Moreno, S. Casado, L. R. González, H. Sawada, J. M. González-Calbet, E. M. Pérez, *Nat. Commun.* **2018**, *9*, 2671, https://doi.org/10.1038/s41467-018-05183-8; c) J. L. Nova-Fernández, D. González-Muñoz, G. Pascual-Coca, M. Cattelan, S. Agnoli, R. Pérez-Ruiz, J. Alemán, S. Cabrera, M. Blanco, *Adv. Funct. Mater.* **2023**, *34*, 2313102, https://doi.org/10.1002/adfm.202313102.

[5] a) A. D. Franklin, M. C. Hersam, H. P. Wong, *Science* **2022**, *378*, 726–732; b) X. Hu, X. Bao, M. Zhang, S. Fang, K. Liu, J. Wang, R. Liu, S. H. Kim, R. H. Baughman, J. Ding, *Adv. Mater.* **2023**, *35*, e2303035, https://doi.org/10.1002/adma.202303035; c) A. K. Feldman, M. L. Steigerwald, X. Guo, C. Nuckolls, *Acc. Chem. Res.* **2008**, *41*, 1731–1741.

[6] a) R. J. Chen, Y. Zhang, D. Wang, H. Dai, *J. Am. Chem. Soc.* **2001**, *123*, 3838–3839; b) A. Star, D. W. Steuerman, J. R. Heath, J. F. Stoddart, *Angew. Chem. Int. Ed.* **2002**, *41*, 2508–2512; c) S. Wang, D. Yu, L. Dai, *J. Am. Chem. Soc.* **2011**, *133*, 5182–5185; d) J. Kong, M. G. Chapline, H. J. Dai, *Adv. Mater.* **2001**, *13*, 1384–1386.

[7] a) A. de Juan, Y. Pouillon, L. Ruiz-González, A. Torres-Pardo, S. Casado, N. Martín, A. Rubio, E. M. Pérez, *Angew. Chem. Int. Ed.* **2014**, *53*, 5394–5400; b) A. López-Moreno, S. Ibáñez, S. Moreno-Da Silva, L. Ruiz-González, N. M. Sabanés, E. Peris, E. M. Pérez, *Angew. Chem. Int. Ed.* **2022**, *61*, e202208189, https://doi.org/10.1002/anie.202208189.

[8] a) S. X. L. Luo, T. M. Swager, *Nat Rev Methods Primers* **2023**, *3*, 72, https://doi.org/10.1038/s43586-023-00255-6; b) Z. Lin, L. C. Beltran, Z. A. De Los Santos, Y. Li, T. Adel, J. A. Fagan, A. R. Hight Walker, E. H. Egelman, M. Zheng, *Science* **2022**, *377*, 535–539; c) J. T. Metternich, J. A. C. Wartmann, L. Sistemich, R. Nissler, S. Herbertz, S. Kruss, *J. Am. Chem. Soc.* **2023**, *145*, 14776–14783; d) Q. Li, Y. Xu, A. Pedersen, M. Wang, M. Zhang, J. Feng, H. Luo, M. M. Titirici, C. R. Jones, *Adv. Funct. Mater.* **2023**, *34*, 2311086, https://doi.org/10.1002/adfm.202311086.

[9] a) D. Tasis, N. Tagmatarchis, A. Bianco, M. Prato, *Chem. Rev.* **2006**, *106*, 1105–1136; b) E. T. Mickelson, C. B. Huffman, A. G. Rinzler, R. E. Smalley, R. H. Hauge, J. L. Margrave, *Chem. Phys. Lett.* **1998**, *296*, 188–194.

[10] a) F. Liang, A. K. Sadana, A. Peera, J. Chattopadhyay, Z. Gu, R. H. Hauge, W. E. Billups, *Nano Lett.* **2004**, *4*, 1257–1260; b) J. Chattopadhyay, A. K. Sadana, F. Liang, J. M. Beach, Y. Xiao, R. H. Hauge, W. E. Billups, *Org. Lett.* **2005**, *7*, 4067–4069.

[11] a) Y. Ying, R. K. Saini, F. Liang, A. K. Sadana, W. E. Billups, *Org. Lett.* **2003**, *5*, 1471–1473; b) Z. Syrgiannis, V. La Parola, C. Hadad, M. Lucío, E. Vázquez, F. Giacalone, M. Prato, *Angew. Chem. Int. Ed.* **2013**, *52*, 6480–6483; c) J. L. Bahr, J. Yang, D. V. Kosynkin, M. J. Bronikowski, R. E. Smalley, J. M. Tour, *J. Am. Chem. Soc.* **2001**, *123*, 6536–6542.

[12] a) J. Chen, M. A. Hamon, H. Hu, Y. Chen, A. M. Rao, P. C. Eklund, R. C. Haddon, *Science* **1998**, *282*, 95–98; b) J. L. Delgado, P. de la Cruz, F. Langa, A. Urbina, J. Casado, J. T. López Navarrete, *Chem. Commun.* **2004**, 1734–1735; c) V. Georgakilas, K. Kordatos, M. Prato, D. M. Guldi, M. Holzinger, A. Hirsch, *J. Am. Chem. Soc.* **2002**, *124*, 760–761; d) X. He, I. Kevlishvili, K. Murcek, P. Liu, A. Star, *ACS Nano* **2021**, *15*, 4833–4844.

[13] a) M. Holzinger, O. Vostrowsky, A. Hirsch, F. Hennrich, M. Kappes, R. Weiss, F. Jellen, *Angew. Chem. Int. Ed.* **2001**, *40*, 4002–4005; b) A. Setaro, M. Adeli, M. Glaeske, D. Przyrembel, T. Bisswanger, G. Gordeev, F. Maschietto, A. Faghani, B. Paulus, M. Weinelt, R. Arenal, R. Haag, S. Reich, *Nat. Commun.* **2017**, *8*, 14281, https://doi.org/10.1038/ncomms14281.

[14] a) J. Aihara, *J. Phys. Chem.* **1994**, *98*, 9773–9776; b) X. Lu, Z. Chen, *Chem. Rev.* **2005**, *105*, 3643–3696.

[15] a) J. Kozma, S. Papp, R. E. Gyurcsányi, *Anal. Chem.* **2022**, *94*, 8249–8257; b) B. Zhao, H. Hu, R. C. Haddon, *Adv. Funct. Mater.* **2004**, *14*, 71–76; c) W. Zhang, J. K. Sprafke, M. Ma, E. Y. Tsui, S. A. Sydlik, G. C. Rutledge, T. M. Swager, *J. Am. Chem. Soc.* **2009**, *131*, 8446–8454; d) H. Li, F. Cheng, A. M. Duft, A. Adronov, *J. Am. Chem. Soc.* **2005**, *127*, 14518–14524.

[16] a) T. Palacin, H. L. Khanh, B. Jousselme, P. Jegou, A. Filoramo, C. Ehli, D. M. Guldi, S. Campidelli, *J. Am. Chem. Soc.* **2009**, *131*, 15394–15402; b) G. Bottari, G. de la Torre, D. M. Guldi, T. Torres, *Chem. Rev.* **2010**, *110*, 6768–6816.

[17] T. Baumgartner, *Acc. Chem. Res.* **2014**, *47*, 1613–1622.

[18] M. F. Rectenwald, J. R. Gaffen, A. L. Rheingold, A. B. Morgan, J. D. Protasiewicz, *Angew. Chem. Int. Ed.* **2014**, *53*, 4173–4176.

[19] a) J. Hilding, E. A. Grulke, Z. George Zhang, F. Lockwood, *J. Dispersion Sci. Technol.* **2003**, *24*, 1–41; b) W. Wenseleers, I. I. Vlasov, E. Goovaerts, E. D. Obraztsova, A. S. Lobach, A. Bouwen, *Adv. Funct. Mater.* **2004**, *14*, 1105–1112.

[20] a) A. Kumar, J. D. Blakemore, *Inorg. Chem.* **2021**, *60*, 1107–1115; b) R. R. Golwankar, T. D. Curry II, C. J. Paranjothi, J. D. Blakemore, *Inorg. Chem.* **2023**, *62*, 9765–9780; c) K. Yamashita, R. Hirokawa, M. Ichikawa, T. Hisanaga, Y. Nagao, R. Takita, K. Watanabe, Y. Kawato, Y. Hamashima, *J. Am. Chem. Soc.* **2022**, *144*, 3913–3924; d) M. Keener, C. Hunt, T. G. Carroll, V. Kampel, R. Dobrovetsky, T. W. Hayton, G. Ménard, *Nature* **2020**, *577*, 652–655.

[21] a) F. Hof, R. A. Schafer, C. Weiss, F. Hauke, A. Hirsch, *Chem. Eur. J.* **2014**, *20*, 16644–16651; b) C. K. Chan, T. E. Beechem, T. Ohta, M. T. Brumbach, D. R. Wheeler, K. J. Stevenson, *J. Phys. Chem. C* **2013**, *117*, 12038–12044; c) M. He, T. M. Swager, *Chem. Mater.* **2016**, *28*, 8542–8549; d) R. Steeno, M. C. Rodríguez González, S. Eyley, W. Thielemans, K. S. Mali, S. De Feyter, *Chem. Mater.* **2020**, *32*, 5246–5255.

[22] E. Linde, S. Mondal, B. Olofsson, *Adv. Synth. Catal.* **2023**, *365*, 2751–2756.

[23] Deposition Numbers 2362498 (for **1**) and 2362499 (for **2**) contain the supplementary crystallographic data for this paper. These data are provided free of charge by the joint Cambridge Crystallographic Data Centre and Fachinformationszentrum KarlsruheAccess Structures service.

[24] a) G. Cavallo, P. Metrangolo, R. Milani, T. Pilati, A. Priimagi, G. Resnati, G. Terraneo, *Chem. Rev.* **2016**, *116*, 2478–2601; b) L. Turunen, M. Erdélyi, *Chem. Soc. Rev.* **2020**, *49*, 2688–2700.

[25] a) G. Gong, S. Lv, J. Han, F. Xie, Q. Li, N. Xia, W. Zeng, Y. Chen, L. Wang, J. Wang, S. Chen, *Angew. Chem. Int. Ed.* **2021**, *60*, 14831–14835; b) N. S. Soldatova, P. S. Postnikov, D. M.

Ivanov, O. V. Semyonov, O. S. Kukurina, O. Guselnikova, Y. Yamauchi, T. Wirth, V. V. Zhdankin, M. S. Yusubov, R. M. Gomila, A. Frontera, G. Resnati, V. Y. Kukushkin, *Chem. Sci.* **2022**, *13*, 5650–5658.

[26] a) K. Gao, N. S. Goroff, *J. Am. Chem. Soc.* **2000**, *122*, 9320–9321; b) D. Cinčić, T. Friščić, W. Jones, *CrystEngComm* **2011**, *13*, 3224–3231, https://doi.org/10.1039/C0CE00699H; c) Y. Xu, J. Viger-Gravel, I. Korobkov, D. L. Bryce, *J. Phys. Chem. C* **2015**, *119*, 27104–27117; d) L. Maugeri, T. Lébl, D. B. Cordes, A. M. Z. Slawin, D. Philp, *J. Org. Chem.* **2017**, *82*, 1986–1995; e) T. A. Schaub, R. Sure, F. Hampel, S. Grimme, M. Kivala, *Chem. Eur. J.* **2017**, *23*, 5687–5691.

[27] A. Bondi, *J. Phys. Chem.* **1964**, *68*, 441–451.

[28] H. Bock, U. Lechner-Knoblauch, P. Hänel, *Chem. Ber.* **1986**, *119*, 3749.

[29] a) D. B. Chesnut, *J. Am. Chem. Soc.* **1998**, *120*, 10504–10510; b) D. B. Chesnut, A. Savin, *J. Am. Chem. Soc.* **1999**, *121*, 2335–2336.

[30] WebCSD search, May 2024.

[31] A. Pénicaud, P. Poulin, A. Derré, E. Anglaret, P. Petit, *J. Am. Chem. Soc.* **2005**, *127*, 8–9, https://doi.org/10.1021/ja0443373.

[32] a) M. S. Dresselhaus, G. Dresselhaus, R. Saito, A. Jorio, *Phys. Rep.* **2005**, *409*, 47–99; b) A. C. Ferrari, D. M. Basko, *Nat. Nanotechnol.* **2013**, *8*, 235–246.

[33] a) J. F. Moulder, W. F. Stickle, W. M. Sobol, K. D. Bomben, in *Handbook of X-Ray Photoelectron Spectroscopy*, **1992**, Perkin–Elmer, pp. 59; b) A. V. N. C. D. Wagner, A. Kraut-Vass, J. W. Allison, C. J. Powell, J. R. Rumble Jr., *NIST Standard Reference Database 20.* **2003**, *Version 3.4 (web version)*.

[34] F. L. Sebastian, F. Becker, Y. Yomogida, Y. Hosokawa, S. Settele, S. Lindenthal, K. Yanagi, J. Zaumseil, *ACS Nano* **2023**, *17*, 21771–21781.

[35] L. Koefoed, K. H. Vase, J. H. Stenlid, T. Brinck, Y. Yoshimura, H. Lund, S. U. Pedersen, K. Daasbjerg, *ChemElectroChem* **2017**, *4*, 3212–3221.

[36] For relevant Hammett constants, see: C. Hansch, A. Leo, R. W. Taft, *Chem. Rev.* **1991**, *91*, 165–195.

[37] The reduction potentials of Ar_2I^+ species have been found to correlate linearly with the Hammett constants of Ar substituents. For a more detailed discussion, see: P. P. Romańczyk, S. S. Kurek, *Electrochim. Acta.* **2020**, *351*, 136404, https://doi.org/10.1016/j.electacta.2020.136404.

[38] Although electronically disfavored, **1** can fragment to yield a small fraction of $[(i\text{-Pr})_3C_6H_2]\bullet$ and $(C_6H_4I)Ph_2P(O)$ upon reduction. The steric bulk of $[(i\text{-Pr})_3C_6H_2]\bullet$ is expected to hinder bond formation at the SWCNT surface, rendering such a pathway unproductive for covalent functionalization. See: a) C. Combellas, D. Jiang, F. Kanoufi, J. Pinson, F. I. Podvorica, *Langmuir* **2009**, *25*, 286–293; b) S. Savagatrup, V. Schroeder, X. He, S. Lin, M. He, O. Yassine, K. N. Salama, X. X. Zhang, T. M. Swager, *Angew. Chem. Int. Ed.* **2017**, *56*, 14066–14070.

[39] L. Daasch, D. Smith, *Anal. Chem.* **1951**, *23*, 853–868.

[40] a) H. Kataura, Y. Kumazawa, Y. Maniwa, I. Umezu, S. Suzuki, Y. Ohtsuka, Y. Achiba, *Synth. Met.* **1999**, *103*, 2555–2558; b) G. Lolli, L. Zhang, L. Balzano, N. Sakulchaicharoen, Y. Tan, D. E. Resasco, *J. Phys. Chem. B* **2006**, *110*, 2108–2115.

[41] Y. Piao, B. Meany, L. R. Powell, N. Valley, H. Kwon, G. C. Schatz, Y. Wang, *Nat. Chem.* **2013**, *5*, 840–845.

[42] a) H.-Y. Ma, L.-F. Tong, Z.-B. Xu, Z.-P. Fang, *Adv. Funct. Mater.* **2008**, *18*, 414–421; b) Y. Guo, C. Bao, L. Song, B. Yuan, Y. Hu, *Ind. Eng. Chem. Res.* **2011**, *50*, 7772–7783.

[43] a) E. Bakker, M. Telting-Diaz, *Anal. Chem.* **2002**, *74*, 2781–2800; b) R. M. Mayall, C. A. Smith, A. S. Hyla, D. S. Lee, C. M. Crudden, V. I. Birss, *ACS Sens.* **2020**, *5*, 2747–2752.

[44] L. Kavan, L. Dunsch, *ChemPhysChem* **2007**, *8*, 974–998.

[45] a) I. Heller, J. Kong, K. A. Williams, C. Dekker, S. G. Lemay, *J. Am. Chem. Soc.* **2006**, *128*, 7353–7359; b) J. Li, P. H. Q. Pham, W. Zhou, T. D. Pham, P. J. Burke, *ACS Nano* **2018**, *12*, 9763–9774; c) I. Heller, J. Kong, H. A. Heering, K. A. Williams, S. G. Lemay, C. Dekker, *Nano Lett.* **2005**, *5*, 137–142.

[46] a) M. L. Gross, M. A. Hickner, *Electrochem. Solid-State Lett.* **2010**, *13*, K5; b) F. Mastrocinque, G. Bullard, J. A. Alatis, J. A. Albro, A. Nayak, N. X. Williams, A. Kumbhar, H. Meikle, Z. X. W. Widel, Y. Bai, A. K. Harvey, J. M. Atkin, D. H. Waldeck, A. D. Franklin, M. J. Therien, *Proc. Natl. Acad. Sci. USA* **2024**, *121*, e2317078121, https://doi.org/10.1073/pnas.2317078121.

[47] D. Bouilly, J. L. Janssen, J. Cabana, M. Côté, R. Martel, *ACS Nano* **2015**, *9*, 2626–2634.

[48] a) Z. Zhang, J. Yan, *Sens. Actuators B* **2014**, *202*, 1058–1064; b) B. L. Huffman, C. L. Donley, J. L. Dempsey, *J. Electrochem. Soc.* **2023**, *170*, 126501; c) G. Tuci, C. Vinattieri, L. Luconi, M. Ceppatelli, S. Cicchi, A. Brandi, J. Filippi, M. Melucci, G. Giambastiani, *Chem. Eur. J.* **2012**, *18*, 8454–8463.

[49] a) M. N. Jackson, Y. Surendranath, *Acc. Chem. Res.* **2019**, *52*, 3432–3441; b) S. E. Braley, J. Xie, Y. Losovyj, J. M. Smith, *J. Am. Chem. Soc.* **2021**, *143*, 7203–7208.

[50] A. Nag, M. K. Singh, C. A. Morrison, J. B. Love, *Angew. Chem. Int. Ed.* **2023**, *62*, e202308356, https://doi.org/10.1002/anie.202308356.

[51] a) S. Moreno-Da Silva, J. I. Martínez, A. Develioglu, B. Nieto-Ortega, L. de Juan-Fernández, L. Ruiz-Gonzalez, A. Picón, S. Oberli, P. J. Alonso, D. Moonshiram, E. M. Pérez, E. Burzurí, *J. Am. Chem. Soc.* **2021**, *143*, 21286–21293; b) S.-H. Lohmann, K. J. Trerayapiwat, J. Niklas, O. G. Poluektov, S. Sharifzadeh, X. Ma, *ACS Nano* **2020**, *14*, 17675–17682.

[52] Y. Li, Y. F. Yuan, Y. Bai, Y. C. Liu, Z. H. Wang, L. M. Li, F. Wu, K. Amine, C. Wu, J. Lu, *Adv. Energy Mater.* **2018**, *8*, 1702781, https://doi.org/10.1002/aenm.201702781.

[53] a) N. B. Bissonnette, N. Bisballe, A. V. Tran, J. A. Rossi-Ashton, D. W. C. MacMillan, *J. Am. Chem. Soc.* **2024**, *146*, 7942–7949; b) D. I. Bugaenko, A. V. Karchava, *Adv. Synth. Catal.* **2023**, *365*, 1893–1900; c) L. Castoldi, A. A. Rajkiewicz, B. Olofsson, *Chem. Commun.* **2020**, *56*, 14389–14392.

Manuscript received: June 27, 2024
Accepted manuscript online: August 1, 2024
Version of record online: ■■, ■■

Research Article

Nanotubes

Y. Pan, D. Baster, D. Käch, J. Reger, L. Wettstein, F. Krumeich, M. El Kazzi, M. J. Bezdek* **e202412084**

Triphenylphosphine Oxide: A Versatile Covalent Functionality for Carbon Nanotubes

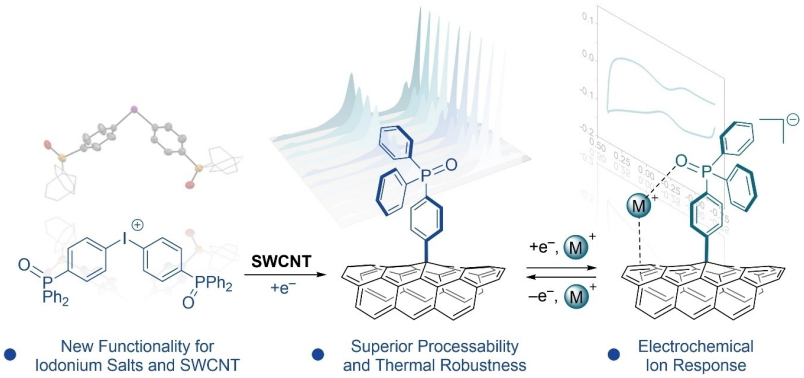

Covalently linking molecules to the surfaces of single-walled carbon nanotubes (SWCNTs) is challenging yet crucial for the versatile function of SWCNTs. We show that the direct covalent SWCNT functionalization with triphenylphosphine oxide yields a new phosphorus-enriched carbon nanomaterial platform exhibiting superior dispersibility, thermal stability and electrochemical ion response.